Structural, electronic, optical, and chiroptical properties of small thiolated gold clusters: The case of Au 6 and Au 8 cores protected with dimer [Au 2(SR) 3] and trimer [Au 3(SR)...

ARTICLE *in* PHYSICAL CHEMISTRY CHEMICAL PHYSICS · APRIL 2012

Impact Factor: 4.49 · DOI: 10.1039/c2cp40643h · Source: PubMed

2 AUTHORS:

Alfredo Tlahuice-Flores
University of Texas at San Antonio
25 PUBLICATIONS **259** CITATIONS
SEE PROFILE

Ignacio L Garzón
Universidad Nacional Autónoma de México
103 PUBLICATIONS **3,023** CITATIONS
SEE PROFILE

PCCP

Cite this: *Phys. Chem. Chem. Phys.*, 2012, **14**, 7321–7329

www.rsc.org/pccp

PAPER

Structural, electronic, optical, and chiroptical properties of small thiolated gold clusters: the case of Au_6 and Au_8 cores protected with dimer $[Au_2(SR)_3]$ and trimer $[Au_3(SR)_4)]$ motifs†

Alfredo Tlahuice and Ignacio L. Garzón*

Received 29th February 2012, Accepted 3rd April 2012
DOI: 10.1039/c2cp40643h

We report results of a theoretical study, based on density functional theory (DFT), on the structural, electronic, optical, and chiroptical properties of small thiolated gold clusters, $[Au_n(SR)_m$ (n = 12–15, 16–20; m = 9–12, 12–16)]. Some of these clusters correspond to those recently synthesized with the surfactant-free method. To study the cluster physical properties, we consider two cluster families with Au_6 and Au_8 cores, respectively, covered with dimer $[Au_2(SR)_3]$ and trimer $[Au_3(SR)_4]$ (CH_3 being the R group) motifs or their combinations. Our DFT calculations show, by comparing the relaxed structures of the $[Au_6[Au_2(SR)_3]_3]^+$, $[Au_6[Au_2(SR)_3]_2[Au_3(SR)_4]]^+$, $[Au_6[Au_2(SR)_3][Au_3(SR)_4]_2]^+$, and $[Au_6[Au_3(SR)_4]_3]^+$ cationic clusters, that there is an increasing distortion in the Au_6 core as each dimer is replaced by a longer trimer motif. For the clusters in the second family, $Au_8[Au_3(SR)_4]_4$, $Au_8[Au_2(SR)_3][Au_3(SR)_4]_3$, $Au_8[Au_2(SR)_3]_2[Au_3(SR)_4]_2$, $Au_8[Au_2(SR)_3]_3[Au_3(SR)_4]$, and $Au_8[Au_2(SR)_3]_4$, a smaller distortion of the Au_8 core is observed as dimer motifs are substituted by trimer ones. An interesting trend emerging from the present calculations shows that as the number of trimer motifs increases in the protecting layer of both Au_6 and Au_8 cores, the average of the interatomic Au(core)–S distances reduces. This shrinkage in the Au(core)–S distances is correlated with an increase of the cluster HOMO–LUMO (H–L) gap. From these results, it is predicted that a larger number of trimer motifs in the cluster protecting layer would induce larger H–L gaps. By analyzing the electronic transitions that characterize the optical absorption and circular dichroism spectra of the clusters under study, it is observed that the molecular orbitals involved are composed of comparable proportions of orbitals corresponding to atoms forming the cluster core and the protecting dimer and trimer motifs.

Introduction

Research on thiolate-protected gold clusters $[Au_n(SR)_m$, SR being a thiolate group] has shown important advances during the last few years mainly due to the success in their crystallization, allowing X-ray total structure determination and further experimental characterization, as well as to the reliability of theoretical studies on their physicochemical properties, using *state of the art* density functional theory calculations.[1–3] The first studies of this type revealed that the structure of the Au_{102}(p-MBA)$_{44}$,[4,5] $[Au_{25}(SC_2H_4Ph)_{18}]^-$,[6–8] and $Au_{38}(SC_2H_4Ph)_{24}$[9,10] clusters is composed of a nearly symmetric Au core (Au_{79}, Au_{13}, and Au_{23}, respectively) protected by N monomer (–RS–Au–SR) and M dimer (–RS–Au–SR–Au–SR) motifs, where (N,M) = (19,2), (0,12), and (3,6), respectively. Other experimental efforts have enabled the synthesis of larger thiolated gold clusters like $Au_{40}(SR)_{24}$,[11] $[Au_{44}(SR)_{28}]^{(2-)}$,[12] $Au_{68}(SR)_{34}$,[13] and $Au_{144}(SR)_{60}$.[14,15] The peculiar structures, composition, and stability of these clusters have been analyzed in terms of the "divide and protect" concept[16] and the shell closing electron rules of the superatom complex (SAC) spherical[5] and nonspherical models,[9] leading to the magic number series: 2, 8, 18, 20, 34, 58,... and 4, 14,..., respectively.

In other studies, smaller gold clusters (~1 nm) protected by glutathione (GSH) were synthesized, size separated, and their precise chemical composition was determined by electrospray ionization mass spectrometry.[17] The nine smallest observed compounds were assigned to $Au_{10}(SG)_{10}$, $Au_{15}(SG)_{13}$, $Au_{18}(SG)_{14}$, $Au_{22}(SG)_{16}$, $Au_{22}(SG)_{17}$, $Au_{25}(SG)_{18}$, $Au_{29}(SG)_{20}$, $Au_{33}(SG)_{22}$,

Instituto de Física, Universidad Nacional Autónoma de México, Apartado Postal 20-364, 01000 México D. F., México.
E-mail: tlahuicef@gmail.com, garzon@fisica.unam.mx

† Electronic supplementary information (ESI) available: Calculated optical absorption spectra of the $[Au_{25}(SR)_{18}]^-$ and $Au_{38}(SR)_{24}$ clusters; histograms of interatomic distances; Kohn–Sham energy diagram levels; tables with the excitation energies, oscillator strengths, atomic orbital contributions, and weights of the electronic transitions; and *xyz* relaxed coordinates of all clusters under study. See DOI: 10.1039/c2cp40643h

and $Au_{39}(SG)_{24}$. These compounds were found to be kinetically trapped intermediates, which on reaction with excess ligands transform into the more stable $Au_{25}(SG)_{18}$ cluster.[17] The optical absorption spectra indicated that the electronic structure of the $Au_n(SG)_m$ compounds is well quantized and size-dependent.[17] It was also found that the $Au_n(SG)_m$ clusters are optically active in the visible and UV spectral range.[18] Except for the case of $[Au_{25}(SG)_{18}]^-$, with enhanced stability in its anionic state ($8e^-$ shell closing count), and with the same structure as the one measured for $[Au_{25}(SC_2H_4Ph)_{18}]^-$,[19] no structural information is yet available for the other glutathione-protected clusters. One difficulty is that even for their charged states, it is not straightforward to apply the shell closing electron rules mentioned above.

A similar study on a polydisperse mixture of gold nanoclusters protected with monolayers of *N*-acetyl-L-cysteine (NAC) reported separated fractions of $Au_{10}(NAC)_{10}$, $Au_{12}(NAC)_9$, $Au_{13}(NAC)_{11}$, $Au_{15}(NAC)_{10}$, $Au_{18}(NAC)_{15}$, $Au_{22}(NAC)_{15}$, $Au_{29}(NAC)_{11}$, $Au_{33}(NAC)_{11}$, and $Au_{39}(NAC)_{11}$, using a matrix-assisted laser desorption time-of flight mass spectrometer (MALDI-TOF-MS).[20] As in the case of glutathione-protected gold clusters described above, there is no structural information on the $Au_n(NAC)_m$ clusters, except for the case of $Au_{12}(NAC)_9$, whose structure may be related to the morphology theoretically obtained for the $[Au_{12}(SR)_9]^+$ cluster (see below).

More recently, the surfactant-free synthesis of other families of small protected gold clusters with core sizes in the Au_{16}–Au_{31} size range and R = CH_2CH_2Ph has been reported.[21] In contrast with the metastability found for the glutathione-protected gold clusters,[17] these complexes show no change in the mass spectrum when reacted with excess thiols, suggesting core stability against etching.[21] The observed new cluster sizes were tentatively classified according to the shell closing electron count, defined by the SAC model.[5] Four series of abundance peaks were found in the nanocluster mixture using MALDI-TOF-MS:[21] $Au_{16}(SR)_{12}$, $Au_{17}(SR)_{13}$, $Au_{18}(SR)_{14}$, $Au_{19}(SR)_{15}$, and $Au_{20}(SR)_{16}$, with a shell closing count of $4e^-$; and $Au_{18}(SR)_{13}$, $Au_{19}(SR)_{14}$, $Au_{20}(SR)_{15}$, $Au_{21}(SR)_{16}$, with a shell closing of $5e^-$. Similarly, two additional series with a shell closing count of $8e^-$ and $10e^-$ were also observed in the MALDI-TOF-MS data: $Au_{26}(SR)_{18}$, $Au_{27}(SR)_{19}$, $Au_{28}(SR)_{20}$; and $Au_{29}(SR)_{19}$, $Au_{30}(SR)_{20}$, $Au_{31}(SR)_{21}$, respectively. Although there have not been additional reports on the characterization of these clusters after size separation, it is significant that the optical absorption spectra of the nanocluster mixture still show sharp features characteristic of small <2 nm clusters.[21] Except for the case of $Au_{20}(SR)_{16}$ (see below), the structures of these surfactant-free synthesized protected gold clusters are also still unknown.

As for the case of unprotected gold clusters, the theoretical study of the physicochemical properties of ligand-protected gold clusters requires previous knowledge of their geometric (stable) structures. Although the procedure to obtain such structures (global structural or dynamical optimization using a quantum mechanical description of all atomic interactions) is well established, and has been used in some particular cases (smaller cluster size regime),[22,23] at present it is still computationally prohibitive to use this approach in a routine way. One way to overcome this technical difficulty is to get the cluster geometry from the X-ray total structure determination, if crystallization has been achieved, as was the case for the Au_{102}(p-MBA)$_{44}$,[4,5] $[Au_{25}(SC_2H_4Ph)_{18}]^-$,[6–8] and $Au_{38}(SC_2H_4Ph)_{24}$[9,10] clusters. If this is not the case, *Aufbau principle*-like or other schemes have to be attempted to propose model structures for thiolated gold clusters.[22–27] One of these approaches was suggested by Tsukuda and co-workers,[28] who based on the already known structures of $Au_{102}(SR)_{44}$ and $[Au_{25}(SR)_{18}]^-$ proposed three *principles* for the construction of candidate cluster structures: (1) a highly symmetric core, (2) more dimer motifs than monomers in the protecting layer of the smaller clusters, (3) the surface atoms of the core have to be fully protected by the terminal thiolates of the motifs.[28] These principles were used to propose a bi-icosahedral core protected by a combination of 3 monomer and 6 dimer motifs for the structure of the $Au_{38}(SR)_{24}$ cluster,[28] which was also independently proposed by Pei *et al.*, using similar arguments.[26] The Tsukuda principles together with the shell closing electron rules from the SAC model have also been useful to suggest structural models of larger thiolated gold clusters like $Au_{40}(SR)_{24}$,[11] $Au_{44}(SR)_{28}$,[29] and $Au_{144}(SR)_{60}$.[30]

The coupling of Tsukuda's three principles with the SAC model was also extended to predict the structure of the smallest thiolated gold complexes.[24] In this case, the $[Au_{12}(SR)_9]^+$ cluster composed of an octahedral core protected with 3 dimer motifs was suggested as a candidate geometry for a cluster with the smallest $2e^-$ shell closing count.[24] This theoretical prediction would be confirmed if further studies are realized on the physicochemical properties of the recently synthesized and isolated $Au_{12}(NAC)_9$ complex.[20] On the other hand, a generalized version of the Tsukuda's principles requiring longer motifs for the construction of the protecting layer, as well as the inclusion of non-spherical shell closing electron counts, were necessary to propose structural models of the already synthesized $Au_{20}(SR)_{16}$ cluster.[31] For this small cluster, a geometry composed of a Au_8 core covered with 4 trimer (–RS–Au–SR–Au–SR–Au–SR) motifs was found as the most viable one, from the good agreement between the calculated and experimental optical absorption spectra.[23,25] The trimer motif, which was already present in the protecting layer of high energy isomers of the $Au_{38}(SR)_{24}$ cluster,[32] was introduced since it has a longer atomic chain that can more easily wrap around gold cores as small as Au_4, Au_6, and Au_8.[23,25] More recently, two other thiolated gold clusters have been synthesized: $Au_{19}(SC_2H_4Ph)_{13}$[33] and $Au_{24}(SC_2H_4Ph)_{20}$.[34] The atomic structure of these clusters has been resolved through theoretical calculations suggesting a structure with a Au_{11} core protected by 2 monomer and 3 dimer motifs for the $Au_{19}(SR)_{13}$ cluster,[27] and an elongated Au_8 core covered with 2 trimer $[Au_3(SR)_4]$ and 2 much longer pentamer $[Au_5(SR)_6]$ motifs for the $Au_{24}(SR)_{20}$ cluster.[35]

In this work, motivated by the experimental results[21] and based on the theoretical approaches discussed above, we propose candidate structures for two families of small thiolated gold clusters: $[Au_n(SR)_m]^+$ (n = 12–15, m = 9–12) and $Au_n(SR)_m$ (n = 16–20, m = 12–16), using quantum mechanical calculations based on density functional theory. The first family corresponds to a series of clusters that satisfy the $2e^-$ shell closing count, which is the smallest one within the spherical SAC model. The second family is related to the one recently synthesized, having a $4e^-$ shell closing count, and already detected in the MALDI-TOF-MS data.[21] In addition, we calculate electronic, optical, and chiroptical properties

of the clusters with the proposed structures to get insight into the physicochemical behavior of small thiolated gold clusters. It is expected that these quantum mechanical calculations provide enough theoretical information, not only to help interpret the experimental results available, but also to look for useful trends in the understanding and possible control of the size-dependent properties displayed by ligand-protected gold clusters.

Computational methodology

In the first stage of this theoretical study, we propose the geometries for two families of small thiolated gold clusters: $[Au_n(SR)_m]^+$ (n = 12–15, m = 9–12), and $Au_n(SR)_m$ (n = 16–20, m = 12–16). For this purpose, we start from the structures already suggested for the $[Au_{12}(SR)_9]^+$ [24] and $Au_{20}(SR)_{16}$ [23,25] clusters, respectively. In the first case, the cluster structure is formed by an octahedral Au_6 core protected by 3 dimer motifs, which can be best represented as $[Au_6[Au_2(SR)_3]_3]^+$, to emphasize the core-protecting layer description of the cluster geometry, implied by the "divide and protect" concept.[16] It should be noticed that the clusters to be studied are in the cationic state in order to satisfy the $2e^-$ shell closing count. On the other hand, the structure already suggested[23,25] for $Au_{20}(SR)_{16}$ consists of an elongated Au_8 core, which can be viewed as two edge-fused tetrahedral Au_4 units, protected by 4 trimer motifs. The stability of this $Au_8[Au_3(SR)_4]_4$ prolate-shape cluster is supported by the $4e^-$ shell closing count that corresponds to a magic number of the nonspherical shell model.[23]

In this work, we generate initial structures for the first family of clusters $[Au_n(SR)_m]^+$ (n = 12–15, m = 9–12), by substituting 1, 2, and 3 dimer motifs of $[Au_6[Au_2(SR)_3]_3]^+$ by 1, 2, and 3 trimer motifs, respectively. With this procedure, we obtain initial structures for the $[Au_6[Au_2(SR)_3]_2[Au_3(SR)_4]]^+$ ($[Au_{13}(SR)_{10}]^+$); $[Au_6[Au_2(SR)_3][Au_3(SR)_4]_2]^+$ ($[Au_{14}(SR)_{11}]^+$); and $[Au_6[Au_3(SR)_4]_3]^+$ ($[Au_{15}(SR)_{12}]^+$) clusters. Similarly, by substituting 1–4 trimer by 1–4 dimer motifs, in the $Au_8[Au_3(SR)_4]_4$ ($Au_{20}(SR)_{16}$) cluster, we obtain the initial structures for the $Au_8[Au_2(SR)_3][Au_3(SR)_4]_3$ ($Au_{19}(SR)_{15}$); $Au_8[Au_2(SR)_3]_2[Au_3(SR)_4]_2$ ($Au_{18}(SR)_{14}$); $Au_8[Au_2(SR)_3]_3[Au_3(SR)_4]$ ($Au_{17}(SR)_{13}$); and $Au_8[Au_2(SR)_3]_4$ ($Au_{16}(SR)_{12}$) clusters. In this way the two families of thiolated gold clusters under study are characterized by an Au_n core, covered with different combinations of M dimer and P trimer motifs: n = 6, (M,P) = (3,0); (2,1); (1,2); (0,3) and n = 8, (M,P) = (4,0); (3,1); (2,2); (1,3); (0,4).

Density functional theory (DFT) within the generalized-gradient approximation (GGA) was used to optimize the structure of each thiolated gold cluster. For this purpose, a local structural relaxation starting from the initial geometries described above, followed by a harmonic vibrational frequency analysis, was performed. The –R group was taken as a methyl radical ($-CH_3$) for computing efficiency. For each cluster size, different isomers with distinct locations and relative orientations (on the surface core) of the dimer and trimer motifs were used for the structural relaxations. All calculations were done using the LAN2DZ ($19\ e^-$) basis set for Au and an all-electron description with a 6-31G(d,p) basis set for S, C, and H, together with the PBE approximation for the exchange–correlation (xc) functional, as implemented in the Gaussian 03 (G03) program package.[36] The choice of the PBE functional is justified since it has been shown that other meta-GGA functionals, such as the non-empirical Tao–Perdew–Staroverov–Scuseria (TPSS) and the M06L one, provide similar trends in the relative energies of gold sulfide nanoclusters.[37] Structural optimizations were carried out without symmetry restrictions, using a force tolerance criterion of 0.01 eV $Å^{-1}$. A similar DFT methodology has been already used to find the three most stable isomers of the $Au_{20}(SCH_3)_{16}$ cluster whose structure provides the best agreement between the calculated and experimental optical absorption spectra.[23]

Time-dependent DFT (TD-DFT), as implemented in G03,[36] was utilized for the study of the optical and chiroptical properties of the thiolated clusters, through the calculation of their excitation energies, and oscillator and rotatory strengths. To calculate the optical absorption and circular dichroism spectra, particularly in the low energy region (1.0–3.5 eV), the lowest 70 excited (singlet) states were considered, using the same xc functional and basis set as for the structural calculations. To test the reliability of the present TD-DFT methodology, a comparison between the calculated optical absorption spectra of the $[Au_{25}(SCH_3)_{18}]^-$ and $Au_{38}(SR)_{24}$ clusters with previous calculations was performed,[7,9] indicating a good agreement, as it is shown in Fig. S1 and S2 in the ESI† section.

Although a higher level of theory[38] may be used to calculate physicochemical properties of some specific ligand-protected gold clusters, in the present study we are interested in using a theoretical methodology reliable enough to obtain useful trends on the size-dependent behavior of the above-mentioned families of small thiolated gold clusters. According to the described successful tests, and the feasibility of the systematic calculations mentioned above, the use of the present methodology is justified.

Results and discussion

Structural properties

The initial structures of the two families of small thiolated gold clusters described in the last section, $[Au_n(SR)_m]^+$ (n = 12–15, m = 9–12) and $Au_n(SR)_m$ (n = 16–20, m = 12–16) were locally optimized to find the most stable configurations. A vibrational analysis was used to confirm that the relaxed structures indeed correspond to true minima of the cluster potential energy surface. Fig. 1 shows the most stable geometries for $[Au_{12}(SCH_3)_9]^+$, $[Au_{13}(SCH_3)_{10}]^+$, $[Au_{14}(SCH_3)_{11}]^+$, and $[Au_{15}(SCH_3)_{12}]^+$, whereas Fig. 2 displays the corresponding configurations for $Au_{16}(SCH_3)_{12}$, $Au_{17}(SCH_3)_{13}$, $Au_{18}(SCH_3)_{14}$, $Au_{19}(SCH_3)_{15}$, and $Au_{20}(SCH_3)_{16}$. All thiolated gold cluster structures were found with C_1 symmetry, considering Au and S atoms, and using a bond length tolerance of 0.1 Å. However, the Au_6 and Au_8 cores resulted with O_h and D_{2d} symmetry, respectively.

One of the effects to be investigated in the present study is what structural changes occur in the small thiolated gold clusters when there are substitutions in the number and type of protecting units (dimer and trimer motifs). It was obtained, by comparing the relaxed structures of $[Au_6[Au_2(SR)_3]_3]^+$, $[Au_6[Au_2(SR)_3]_2[Au_3(SR)_4]]^+$, $[Au_6[Au_2(SR)_3][Au_3(SR)_4]_2]^+$, and $[Au_6[Au_3(SR)_4]_3]^+$ clusters, that there is an increasing distortion in the Au_6 core as each dimer motif is replaced by a

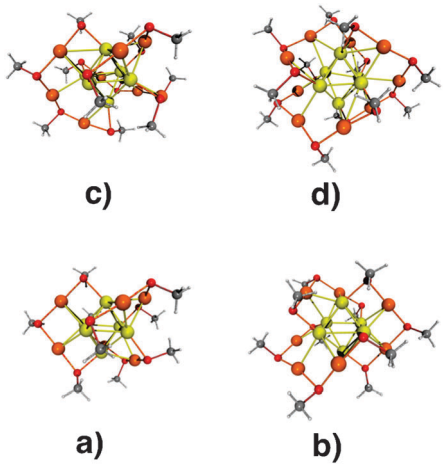

Fig. 1 Most stable structures of the (a) $[Au_{12}(SCH_3)_9]^+$; (b) $[Au_{13}(SCH_3)_{10}]^+$; (c) $[Au_{14}(SCH_3)_{11}]^+$; and (d) $[Au_{15}(SCH_3)_{12}]^+$ clusters. Color of atoms is as follows: Au(core) in yellow, Au(I) [in the dimer and trimer motifs] in orange, S in red, C in gray, H in white.

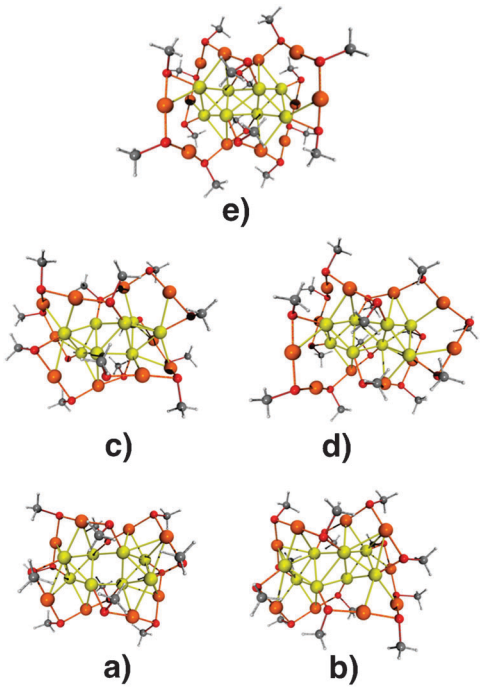

Fig. 2 Most stable structures of the (a) $Au_{16}(SCH_3)_{12}$; (b) $Au_{17}(SCH_3)_{13}$; (c) $Au_{18}(SCH_3)_{14}$; (d) $Au_{19}(SCH_3)_{15}$; and (e) $Au_{20}(SCH_3)_{16}$ clusters. Color of atoms is defined in Fig. 1.

longer trimer one. This increasing structural distortion in the Au_6 core can be appreciated in Fig. S3 (ESI†) that shows a broad range of values (2.68–2.98 Å) of the 12 Au(core)–Au(core) [Au(core) being an Au atom forming the cluster core] interatomic nearest-neighbor distances in the octahedral core for the 4 thiolated gold clusters. A similar increasing dispersion in the values of the Au(core)–Au(I) [Au(I) being a gold atom forming a dimer or trimer motif] distances (2.88–3.58 Å) is also shown in Fig. S3 (ESI†). In contrast, the Au(core)–S and Au(I)–S distances in the 4 thiolated gold clusters are distributed in a much narrower band (2.36–2.42 Å), as it is also shown in Fig. S3 (ESI†).

Fig. S4 (ESI†) displays the Au(core)–Au(core), Au(core)–Au(I), Au(core)–S, and Au(I)–S nearest neighbor distances in the $Au_8[Au_3(SR)_4]_4$ $Au_8[Au_2(SR)_3][Au_3(SR)_4]_3$, $Au_8[Au_2(SR)_3]_2$-$[Au_3(SR)_4]_2$, $Au_8[Au_2(SR)_3]_3[Au_3(SR)_4]$, and $Au_8[Au_2(SR)_3]_4$ clusters. In these cases, a smaller distortion of the Au_8 core is observed as dimer motifs are substituted by trimer ones. For example, the 12 Au(core)–Au(core) nearest-neighbor distances of the two Au_4 tetrahedral units are distributed in a narrower band (2.76–2.90 Å) than that observed for the Au_6 core, although the two Au–Au distances connecting the tetrahedral cores are in the range of 3.05–3.15 Å. On the other hand, the Au(core)–Au(I), Au(core)–S, and Au(I)–S distances are similarly distributed in the two families of thiolated gold clusters, although the Au(core)–Au(I) distances are more dispersed than the Au(core)–Au(core), Au(core)–S, and Au(I)–S ones. An overall trend emerging from the present structural analysis shows that as the number of trimer motifs increases in the protecting layer of both Au_6 and Au_8 cores, the average of the Au(core)–S distances reduces. This shrinkage in the Au(core)–S distances, shown in Fig. S3 and S4 (ESI†), is related with an interesting effect on the electronic properties of the two cluster families (see below).

Further analysis of the results shown in Fig. S3 and S4 (ESI†) indicates that the largest Au_6 core distortion is generated when it is covered by 3 trimer motifs in the $[Au_{15}(SCH_3)_{12}]^+$ cluster, as compared with the case in which no significant distortion is obtained for the octahedral core when it is only protected by dimers, as in the case of the $[Au_{12}(SCH_3)_9]^+$ cluster. This effect may be due to a larger strain accumulation in the compact Au_6 core when it is protected by the longer trimer motifs. The absence of distortion when only dimer motifs protect the Au_6 core was also reported by Jiang *et al.*,[24] indicating that the O_h symmetry is only reduced to D_{3d} (within 0.06 Å tolerance) upon relaxation with the thiol ligands, in agreement with our results. In contrast, this increasing core structural distortion due to trimers is not observed in the Au_8 cores, indicating that the elongated structure can relieve more efficiently the additional strain induced by the longer trimer chains. In this case, the two edge-fused Au_4 tetrahedra forming the elongated Au_8 core may undergo relative rotations and extensions with respect to the longitudinal axis, as more trimer motifs protect the cluster surface. On the other hand, the largest Au_8 core distortion is observed for the $Au_{18}(SCH_3)_{14}$ cluster, where 2 dimer and 2 trimer motifs cover simultaneously the core surface.[39] In fact, the structure of the Au_8 core of this cluster, which was found to be with the highest relative abundance in the surfactant-free synthesis,[21] cannot be viewed as two edge-fused tetrahedral Au_4 units, as was found for the core of $Au_{20}(SCH_3)_{16}$.[23]

The simulated X-ray diffraction (XRD) patterns of the two families, displayed in Fig. 3, confirm the structural trends mentioned above. For $[Au_n(SR)_m]^+$ (n = 12–15, m = 9–12), the XRD patterns show a strong peak at around 4 nm^{-1}, whereas for $Au_n(SR)_m$ (n = 16–20, m = 12–16), the most intense peak is centered at 3.8 nm^{-1}, mainly reflecting the different geometries of the octahedral and two-tetrahedral cores. It is also notorious from Fig. 3 that the dispersion in the position of the maximum of the main peak is larger for the clusters with the octahedral Au_6 core than that displayed for the clusters with the elongated Au_8 core. This behavior is consistent with the larger distortion occurring in the octahedral

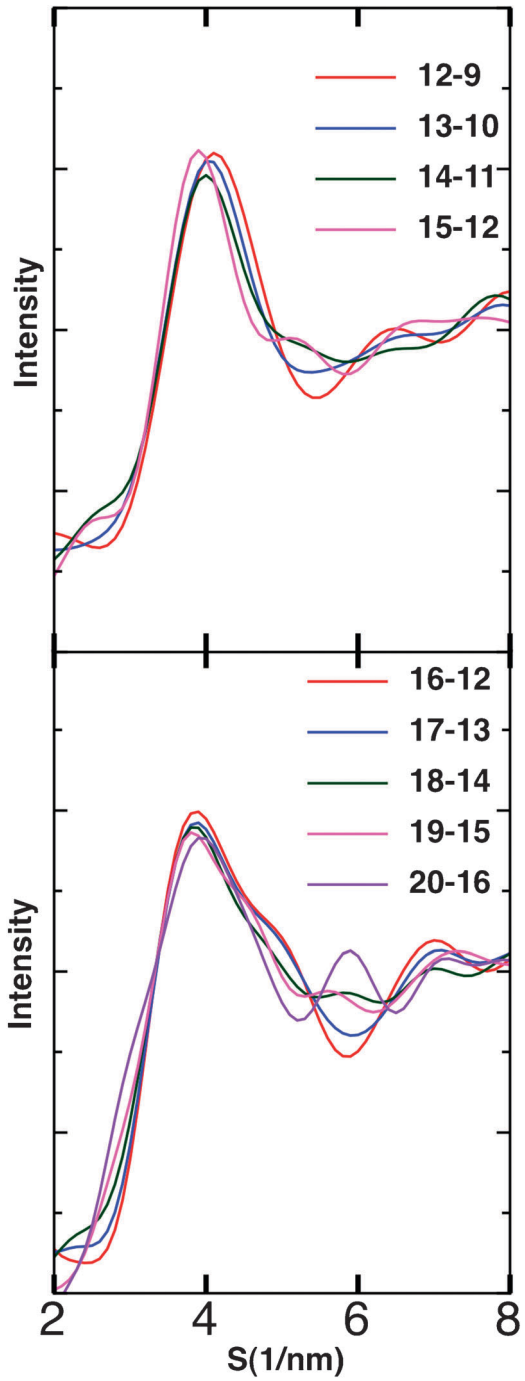

Fig. 3 Simulated XRD patterns. Top panel: $Au_{12}(SCH_3)_9^+$, $Au_{13}(SCH_3)_{10}^+$, $Au_{14}(SCH_3)_{11}^+$, and $Au_{15}(SCH_3)_{12}^+$. Bottom panel: $Au_{16}(SCH_3)_{12}$, $Au_{17}(SCH_3)_{13}$, $Au_{18}(SCH_3)_{14}$, $Au_{19}(SCH_3)_{15}$, and $Au_{20}(SCH_3)_{16}$.

core, as dimer motifs are substituted by the longer trimer ones mentioned above. The distinct lineshapes of the XRD patterns in the range of 2–3 nm^{-1} for the two families of protected clusters are a signature of the different arrangements that the dimer and trimer motifs produce in the protecting layer of the octahedral and elongated cores. On the other hand, the different lineshapes of the XRD patterns for $s > 4$ nm^{-1} are related with higher order diffraction behavior of the distinct protected cluster structures.

Electronic properties

The variation in electronic properties of the two cluster families as a consequence of different structural patterns in the protecting layer was studied by analyzing the HOMO–LUMO (H–L) gap values as well as the atomic orbital components of the molecular orbitals (MO), which would be involved in low-energy electronic transitions. Table 1 shows the H–L values for all clusters studied, including the one obtained for the well-known $[Au_{25}(SR)_{18}]^-$ anionic cluster. The H–L gaps calculated in this work for $Au_{20}(SR)_{16}$ and $[Au_{25}(SR)_{18}]^-$ are in good agreement with previous calculations,[8,23,25] however the calculated value (1.49 eV) for the $[Au_{12}(SCH_3)_9]^+$ cluster is smaller than that obtained (1.70 eV) by Jiang and coworkers.[24] One possible reason for this discrepancy would be related with the lower symmetry (C_1) of the structure calculated in this work, as compared with the higher symmetry one (C_3) obtained by Jiang *et al.*[24] On the other hand, it is also known that the TPSS functional used by Jiang *et al.*[24] gives a slightly higher H–L gap than the PBE one, for the same cluster structures.

An interesting trend emerging from the values displayed in Table 1 indicates that the H–L gap increases, as more trimer motifs are present in the protecting layer of both Au_6 and Au_8 cores. This behavior is more evident in the $Au_n(SR)_m$ (n = 16–20, m = 12–16) cluster family, where the H–L gap increases from 1.41 eV in $Au_{16}(SR)_{12}$ with no trimer motifs in the protecting layer, up to 2.26 eV in $Au_{20}(SR)_{16}$ when there are 4 trimer motifs covering the Au_8 elongated core. This effect points out that there should be a relationship between the ligand layer structure and the H–L gap in small thiolated gold clusters. In fact, this effect has been discussed by Pei *et al.*,[35] for larger thiol-protected gold clusters, suggesting that a decrease of the H–L gap is related with an increase of the average bond length of Au(core)–S. We have confirmed, by using the data shown in Fig. S1 and S2 (ESI†) for the Au(core)–S distances, that indeed the rise of the H–L gaps, as the number of trimer motifs increases in the ligand-protecting layer of the Au_6 and Au_8 cores, is related with a shrinkage in the average of the Au(core)–S distances (see Fig. 4). This result, indicating that the factor that controls the H–L gap is the average bond length between the Au(core) and S atoms, which according to the present results, depends on the number of trimer motifs, expands to the small cluster size regime a similar conclusion obtained by Pei *et al.*[35] for thiolated gold clusters up to $Au_{102}(SR)_{44}$ and $Au_{144}(SR)_{60}$.

We have investigated the relative stability among the cationic and neutral clusters by calculating at the same level of theory the total energies involved in the reactions $[Au_n(SR)_m]^+ + 1/4(AuSR)_4 \rightarrow [Au_{n+1}(SR)_{m+1}]^+$ (n = 12–14; m = 9–11); and $Au_n(SR)_m + 1/4(AuSR)_4 \rightarrow Au_{n+1}(SR)_{m+1}$ (n = 16–19; m = 12–15), where $(AuSR)_4$ is the well-known cyclic tetramer. Our results show that for both cluster families the relative stability increases with size, however, while the difference in energy between the (n = 15, m = 12) and (n = 12, m = 9) cationic clusters is 0.77 eV, a much higher relative stability (1.33 eV) was obtained for the (n = 20, m = 16) neutral cluster, as compared with the (n = 16, m = 12) one. These results might be correlated with the much higher increment with cluster size of the calculated H–L gap values obtained for the cluster family based on the Au_8 core, as compared with the smaller increment

Table 1 Number of dimer and trimer motifs and HOMO–LUMO gaps of the thiolated gold clusters

Cluster	Short notation	Staple motifs dimer/trimer	HOMO–LUMO gap/eV
$[Au_6@[Au_2(SCH_3)_3]_3]^+$	$Au_{12}(SCH_3)_9^+$	3/0	1.49
$[Au_6@[Au_2(SCH_3)_3]_2[Au_3(SCH_3)_4]]$	$Au_{13}(SCH_3)_{10}^+$	2/1	1.48
$[Au_6@[Au_2(SCH_3)_3][Au_3(SCH_3)_4]_2]^+$	$Au_{14}(SCH_3)_{11}^+$	1/2	1.49
$[Au_6@[Au_3(SCH_3)_4]_3]^+$	$Au_{15}(SCH_3)_{12}^+$	0/3	1.56
$Au_8@[Au_2(SCH_3)_3]_4$	$Au_{16}(SCH_3)_{12}$	4/0	1.41
$Au_8@[Au_2(SCH_3)_3]_3[Au_3(SCH_3)_4]$	$Au_{17}(SCH_3)_{13}$	3/1	1.51
$Au_8@[Au_2(SCH_3)_3]_2[Au_3(SCH_3)_4]_2$	$Au_{18}(SCH_3)_{14}$	2/2	1.63
$Au_8@[Au_2(SCH_3)_3][Au_3(SCH_3)_4]_3$	$Au_{19}(SCH_3)_{15}$	1/3	1.80
$Au_8@[Au_3(SCH_3)_4]_4$	$Au_{20}(SCH_3)_{16}$	0/4	2.26
$[Au_{13}@[Au_2(SCH_3)_4]_6]^-$	$Au_{25}(SCH_3)_{18}^-$	6/0	1.25

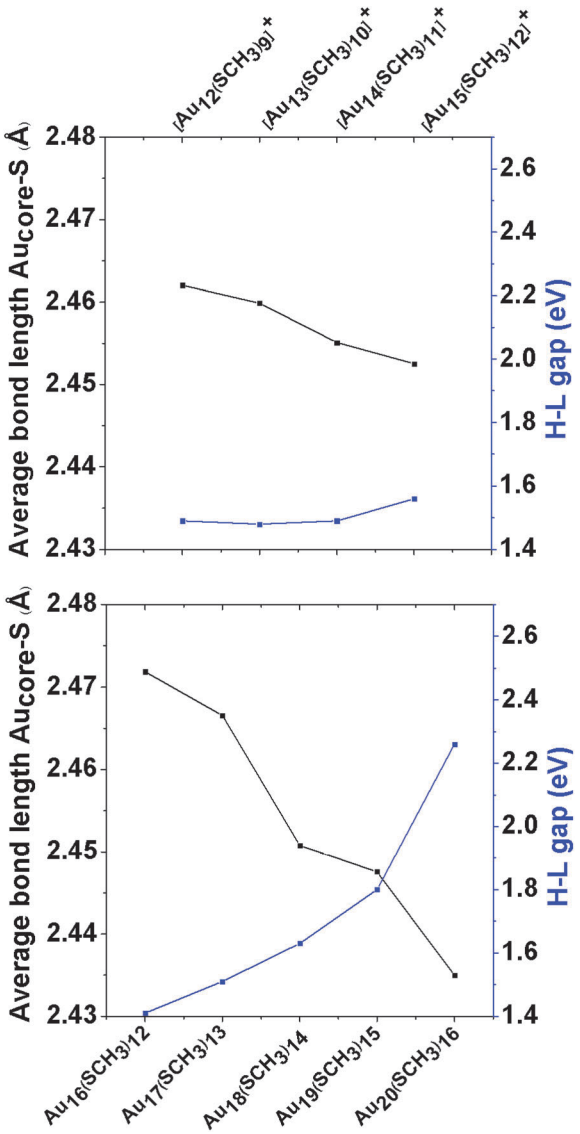

Fig. 4 Correlation between the HOMO–LUMO gap and the average bond length of the Au(core)–S. Top panel: $Au_{12}(SCH_3)_9^+$, $Au_{13}(SCH_3)_{10}^+$, $Au_{14}(SCH_3)_{11}^+$, and $Au_{15}(SCH_3)_{12}^+$. Bottom panel: $Au_{16}(SCH_3)_{12}$, $Au_{17}(SCH_3)_{13}$, $Au_{18}(SCH_3)_{14}$, $Au_{19}(SCH_3)_{15}$, and $Au_{20}(SCH_3)_{16}$.

in the corresponding values calculated for the cationic clusters based on the Au_6 core. Moreover, this relation between the relative stabilities among the structures of anionic and neutral clusters with their calculated H–L gaps could provide insight in order to explain the weaker correlation between the Au(core)–S distances and the H–L gaps obtained for the Au_6 core case, shown in the top panel of Fig. 4.

Additional insights into the electronic properties of small thiolated gold clusters can be extracted by analyzing their Kohn–Sham MO energy level diagram displayed in Fig. S5 and S6 (ESI†). Of particular interest are the atomic orbital components [Au(core), Au(I), and S] of the MO located around the H–L region that are reported in Tables S1 and S2 (ESI†). One of the questions to be investigated is if the MO with energies in the H–L gap region are mainly composed of orbitals coming from the Au(core) atoms, as was obtained for the larger anionic $[Au_{25}(SR)_{18}]^-$ cluster,[7] or a different behavior occurs for the smaller thiolated gold clusters studied in this work.

As a general trend, Table S1 (ESI†) shows that for $[Au_n(SR)_m]^+$ (n = 12–15, m = 9–12) clusters with an octahedral core, the HOMOs have a larger contribution from the S atoms as compared with the one coming from the Au(core) atoms. On the other hand, the LUMOs are mainly composed of orbitals coming from the Au(core) atoms. Although the contribution from the Au(I) atoms forming the dimer and trimer motifs is in general smaller than that coming from the Au(core) and S atoms in the whole H–L region, when it is added to the S atoms contribution, the HOMO and the orbitals with lower energy are mainly composed of orbitals from atoms forming the protecting layer, whereas the LUMO and orbitals with higher energy are composed of a similar proportion of core and protecting layer atoms.

For $Au_n(SR)_m$ (n = 16–20, m = 12–16) clusters, Table S2 (ESI†) shows a slightly different behavior, indicating an increase of the contribution from the S atoms to the composition of the HOMO, as the number of trimer motifs rises from zero in the $Au_{16}(SR)_{12}$ cluster to four in the $Au_{20}(SR)_{16}$ one. This increment is in contrast with a decrease in the contribution of the Au(core) atoms to such orbital for the same sequence of cluster sizes. These variations produce HOMO and orbitals with lower energy with larger contributions from the atoms forming the ligand layer, with respect to the Au(core) contribution, as there is a rise in the number of trimer motifs. On the other hand, the LUMO and orbitals with higher energy show a similar contribution from atoms in the protecting layer and the Au_8 core.

The above trends suggest that for the small thiolated gold clusters studied here, there would not be a clear separation between the electronic properties of the core and the protecting layer, as was found for the larger anionic $[Au_{25}(SR)_{18}]^-$ cluster.[7]

Optical and chiroptical properties

An important question in the present investigation is what consequences the trends in the structural and electronic properties mentioned above will have on the optical and chiroptical properties of the two families of small thiolated gold clusters under study. Fig. 5 and 6 display the calculated optical absorption (left panel) and the electronic circular dichroism (right panel) spectra for the $[Au_n(SR)_m]^+$ (n = 12–15, m = 9–12) and $Au_n(SR)_m$ (n = 16–20, m = 12–16) clusters, respectively. These spectra show the energy location and the relative intensities of the transitions (color bars) between MO shown in Fig. S5 and S6 (ESI†), as well as their Gaussian broadening (0.1 eV, black curve). The more intense peaks in the optical absorption spectra have been labeled according to the different groups of characteristic transitions that are also shown in Tables S1 and S2 (ESI†). The optical absorption spectra calculated in this work for the $[Au_{12}(SR)_9]^+$ and $Au_{20}(SR)_{16}$ clusters are in good agreement with previous calculations[24,26] indicating the reliability of our methodology. Similarly, the calculated optical absorption and

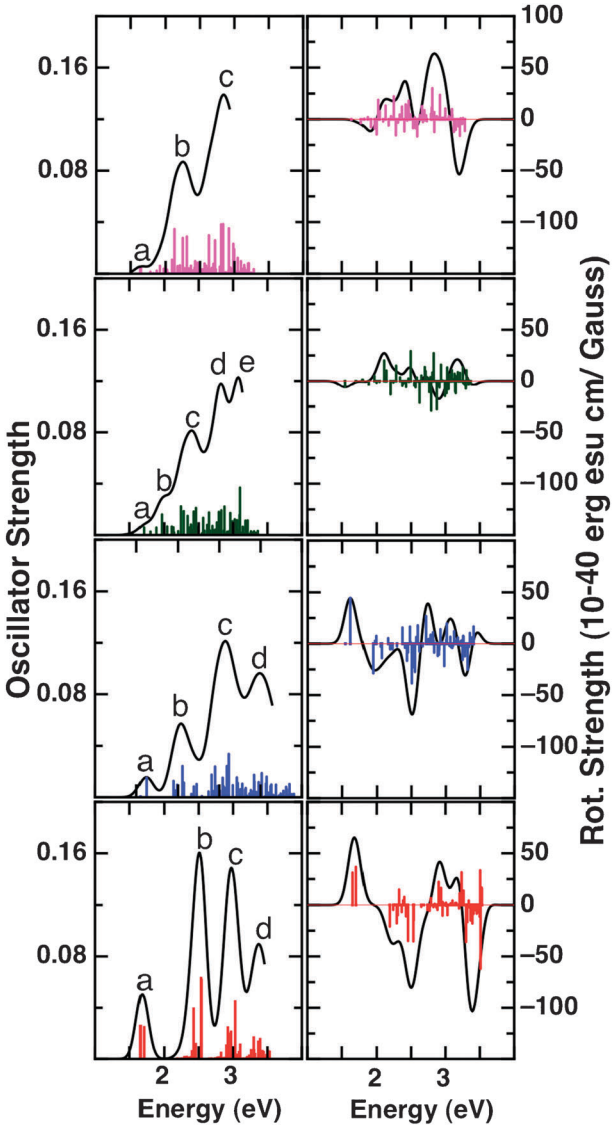

Fig. 5 Calculated oscillator (left column) and rotatory (right column) strengths for the clusters based on the Au_6 core. Colors indicate different cluster sizes: red is 12-9, blue is 13-10, green is 14-11 and pink is 15-12. A Gaussian broadening of 0.1 eV was used to generate the lineshape (black curve) of the corresponding optical absorption and circular dichroism spectra. Labels (a–e) in peaks are correlated with groups of transitions described in Table S1 (ESI†).

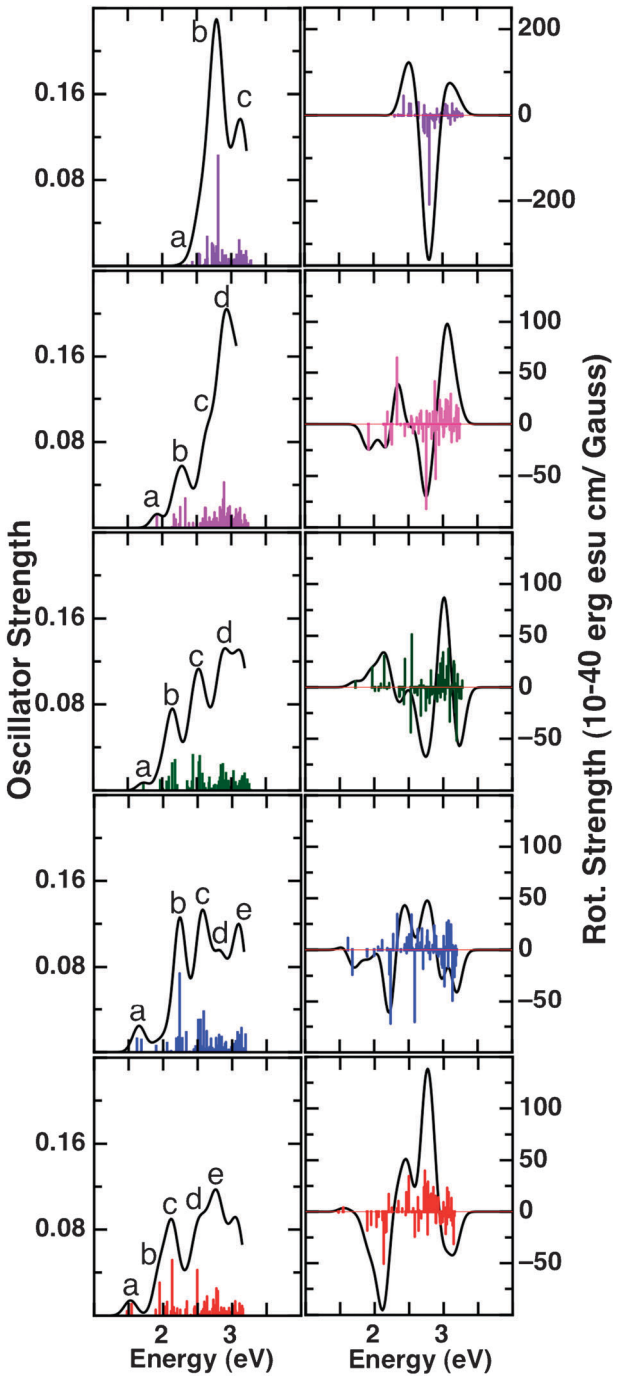

Fig. 6 Calculated oscillator (left column) and rotatory (right column) strengths for the clusters based on the Au_8 core. Colors indicate different cluster sizes: red is 16-12, blue is 17-13, green is 18-14, pink is 19-15, and violet is 20-16. A Gaussian broadening of 0.1 eV was used to generate the lineshape (black curve) of the corresponding optical absorption and circular dichroism spectra. Labels (a–e) in peaks are correlated with groups of transitions described in Table S2 (ESI†).

electronic circular dichroism spectra of the $Au_{18}(SR)_{14}$ cluster, recently reported by us,[39] have been found in good agreement with the experimental measurements on glutathione-protected $Au_{18}(SG)_{14}$ clusters.[18]

As a general trend, broadening of both the optical and chiroptical spectra is found as the cluster size increases. For example, the more structured lineshape in the spectra of $[Au_{12}(SR)_9]^+$ and $Au_{16}(SR)_{12}$ is evident from Fig. 5 and 6, as compared with a much broader lineshape of the larger $[Au_{15}(SR)_{12}]^+$ and $Au_{20}(SR)_{16}$ clusters. This behavior is notorious since it was not expected to find this size effect in two families of ligand-protected clusters that are considered within the small cluster size regime.

The main insight that may be obtained by analyzing the calculated transitions that characterize the whole optical absorption spectra of the clusters under study is related with the fact that the MO involved are composed of comparable proportions of orbitals corresponding to atoms forming the cluster core as well as to atoms in the protecting dimer and trimer motifs. This behavior can be appreciated from Tables S1 and S2 (ESI†) that show excitation energies, oscillator strengths, type of electronic transitions, and relative contributions (in percentage) of the atomic orbitals to each MO for peaks a–e of the two cluster families under study. This result is particularly relevant for transitions (peaks with labels a and b) in the low-energy region (1.5–2.5 eV), since previous calculations on larger clusters like $[Au_{25}(SR)_{18}]^-$ [7,40] indicated that in such energy region, the orbitals mainly coming from the Au core atoms contributed to such transitions. Again, this behavior is a peculiarity of the small cluster size regime characterizing the two cluster families under study, which was anticipated from the discussion of their electronic properties mentioned above.

The distinct lineshapes of the optical spectra for the two cluster families shown in Fig. 5 and 6 illustrate their strong dependence on the cluster structure. In these cases, it is striking to notice how different the spectra lineshapes may be when octahedral Au_6 or elongated Au_8 cores are covered with different number and combinations of dimer and trimer motifs. For example, the depression through a blue shift of the first peak (with label a) is notorious as the number of trimer motifs increases in the two cluster families. In fact, the strong sensitivity of the optical absorption to the cluster morphology has been used for the cluster structure assignment through a comparison between calculated and measured spectra.[7–9,22–27,35,38–40]

Interesting trends may also be extracted from the circular dichroism (CD) spectra shown in the right columns of Fig. 5 and 6. As expected, the chirality characterizing the most stable cluster structures, with C_1 symmetry, induces a nonzero CD signal for all clusters studied. The distinct CD lineshapes confirm the strong sensitivity of the optical activity to the chiral cluster structure. At present, there are no experimental results on the optical activity for the clusters studied in this work that would allow a comparison and possible structure assignment, except for the case of the calculated CD spectrum of $Au_{18}(SR)_{14}$,[39] which has been found in good agreement with the measurements obtained for the glutathione-protected $Au_{18}(SG)_{14}$ cluster.[18]

Despite the small size of the compounds under investigation, the overall calculated CD intensities are of the same order of magnitude as those reported for larger $[Au_{25}(SR)_{18}]^-$,[41] $Au_{38}(SR)_{24}$,[9] and $Au_{24}(SR)_{20}$ clusters.[35] However, it is worth noting the much higher CD intensity (a strong negative peak at around 2.8 eV) displayed by $Au_{20}(SR)_{16}$, as compared with the signals coming from other clusters within the same family. This effect would not be related with a higher symmetry of that isomer (with C_1 symmetry), as was found for the relative intensities between chiral isomers of $Au_{38}(SR)_{24}$[9] and $Au_{24}(SR)_{20}$.[35] On the other hand, by looking at the atomic orbital components of the MO involved in transition at around 2.8 eV, it is found that the S and Au(I) atoms, forming the protecting motifs, provide the major contribution.

As in the case of the optical absorption spectra, an overall trend emerging from the analysis of the electronic transitions giving rise to the CD spectra indicates that the MO involved are composed of comparable proportions of orbitals corresponding to atoms forming the cluster core as well as from the protecting dimer and trimer motifs. This behavior suggests that the origin of the optical activity in the two cluster families under study is related with the chirality of the whole ligand-protected cluster, instead of an intrinsic chirality of the Au_6 and Au_8 cores, or the formation of chiral symmetry patterns from the dimer or trimer motifs arrangement on achiral Au_6 and Au_8 cores. The present calculations suggest the existence of a global cluster chirality, which would be a specific characteristic of smaller (molecular-like) ligand-protected clusters, which is in contrast with other mechanisms that explain the optical activity found for larger $[Au_{25}(SG)_{18}]^-$ and $Au_{38}(SR)_{24}$ chiral clusters.[9,41–43]

Summary

Calculations on structural, electronic, optical, and chiroptical properties for two families of small thiolated gold clusters: $[Au_n(SR)_m]^+$ (n = 12–15, m = 9–12) and $Au_n(SR)_m$ (n = 16–20, m = 12–16), using quantum mechanical calculations based on density functional theory have been presented. The predicted structures correspond to Au_6 and Au_8 cores protected by different combinations of dimer and trimer motifs. Our calculations show, by comparing the relaxed structures of the $[Au_6[Au_2(SR)_3]_3]^+$, $[Au_6[Au_2(SR)_3]_2[Au_3(SR)_4]]^+$, $[Au_6[Au_2(SR)_3][Au_3(SR)_4]_2]^+$, and $[Au_6[Au_3(SR)_4]_3]^+$ clusters, that there is an increasing distortion in the Au_6 core as dimers are replaced by longer trimer motifs. For the clusters in the second family, $Au_8[Au_3(SR)_4]_4$ $Au_8[Au_2(SR)_3][Au_3(SR)_4]_3$, $Au_8[Au_2(SR)_3]_2[Au_3(SR)_4]_2$, $Au_8[Au_2(SR)_3]_3[Au_3(SR)_4]$, and $Au_8[Au_2(SR)_3]_4$, a smaller distortion of the Au_8 core is observed as dimer motifs are substituted by trimer ones.

An important result obtained from the calculated cluster structural properties shows that as the number of trimer motifs increases in the protecting layer of both Au_6 and Au_8 cores, the average of the interatomic Au(core)–S distances reduces. This shrinkage in the averaged Au(core)–S distances can be correlated with an increase of the H–L gap, extending a similar trend recently obtained for larger thiolated gold clusters.[35] The present theoretical results, which predict that a larger number of trimer motifs on the cluster protecting layer would induce larger H–L gaps, may be useful for experimental groups working in the design and control of optical and chiroptical properties of metal clusters.

On the other hand, the main insight obtained by analyzing the calculated transitions that characterize the optical absorption and circular dichroism spectra of the clusters under study indicates that the MO involved are composed of comparable proportions of orbitals corresponding to atoms forming the cluster core as well as to atoms in the protecting dimer and trimer motifs. This type of behavior would be a specific characteristic of smaller (molecular-like) ligand-protected clusters, as compared with that found for larger thiolated clusters like $[Au_{25}(SR)_{18}]^-$.[7,40]

In summary, it is expected that the present results motivate further synthesis, size separation, and physicochemical characterization of small chiral thiolated gold clusters, to confirm the predicted trends and properties, and to prove the existence of the longer U-shaped (RS–Au–SR–Au–SR–Au–SR) trimer motifs, as protecting units of ligand-protected gold clusters.

We acknowledge support from Conacyt-México under Project 80610. Calculations were done using resources from the Supercomputing Center DGTIC-UNAM.

Notes and references

1 R. Jin, *Nanoscale*, 2010, **2**, 343; H. Häkkinen and R. L. Whetten, *J. Phys. Chem. C*, 2010, **114**, 15877.
2 R. Tsunoyama, H. Tsunoyama, P. Pannopard, J. Limtrakul and T. Tsukuda, *J. Phys. Chem. C*, 2010, **114**, 16004.
3 J. Akola, K. A. Kacprzak, O. Lopez-Acevedo, M. Walter, H. Grönbeck and H. Häkkinen, *J. Phys. Chem. C*, 2010, **114**, 15986.
4 P. D. Jadzinsky, G. Calero, C. J. Ackerson, D. A. Bushnell and R. D. Kornberg, *Science*, 2007, **318**, 430.
5 M. Walter, J. Akola, O. Lopez-Acevedo, P. D. Jadzinsky, G. Calero, C. J. Ackerson, R. L. Whetten, H. Grönbeck and H. Häkkinen, *Proc. Natl. Acad. Sci. U. S. A.*, 2008, **105**, 9157.
6 M. W. Heaven, A. Dass, P. S. White, K. M. Holt and R. W. Murray, *J. Am. Chem. Soc.*, 2008, **130**, 3754.
7 M. Zhu, C. M. Aikens, F. J. Hollander, G. C. Schatz and R. Jin, *J. Am. Chem. Soc.*, 2008, **130**, 5883.
8 J. Akola, M. Walter, R. L. Whetten, H. Häkkinen and H. Grönbeck, *J. Am. Chem. Soc.*, 2008, **130**, 3756.
9 O. Lopez-Acevedo, H. Tsunoyama, T. Tsukuda, H. Häkkinen and C. M. Aikens, *J. Am. Chem. Soc.*, 2010, **132**, 8210.
10 H. Qian, W. T. Eckenhoff, Y. Zhu, T. Pintauer and R. Jin, *J. Am. Chem. Soc.*, 2010, **132**, 8280.
11 H. Qian, Y. Shu and R. Jin, *J. Am. Chem. Soc.*, 2010, **132**, 4583.
12 R. C. Price and R. L. Whetten, *J. Am. Chem. Soc.*, 2005, **127**, 13750.
13 A. Dass, *J. Am. Chem. Soc.*, 2009, **131**, 11666.
14 C. A. Fields-Zinna, R. Sardar, C. A. Beasley and R. W. Murray, *J. Am. Chem. Soc.*, 2009, **131**, 16266.
15 H. Qian and R. Jin, *Nano Lett.*, 2009, **9**, 4083.
16 H. Häkkinen, M. Walter and H. Grönbeck, *J. Phys. Chem. B*, 2006, **110**, 9927.
17 Y. Negishi, K. Nobusada and T. Tsukuda, *J. Am. Chem. Soc.*, 2005, **127**, 5261; Y. Negishi, Y. Takasugi, S. Sato, H. Yao, K. Kimura and T. Tsukuda, *J. Phys. Chem. B*, 2006, **110**, 12219; Y. Shichibu, Y. Negishi, H. Tsunoyama, M. Kanehara, T. Teranishi and T. Tsukuda, *Small*, 2007, **3**, 835.
18 T. Tsukuda, H. Tsunoyama and Y. Negishi, in *Metal Nanoclusters in Catalysis and Materials Science: The Issue of Size Control*, ed. B. Corain, G. Schmid and M. Toshima, Elsevier, Amsterdam, 2008, p. 373.
19 Z. Wu, C. Gayathri, R. R. Gil and R. Jin, *J. Am. Chem. Soc.*, 2009, **131**, 6535.
20 Y. Zhang, S. Shuang, C. Dong, C.-K. Lo, M.-C. Paau and M. M. F. Choi, *Anal. Chem.*, 2009, **81**, 1676.
21 S. M. Reilly, T. Krick and A. Dass, *J. Phys. Chem. C*, 2010, **114**, 741.
22 D. E. Jiang, M. L. Tiago, W. D. Luo and S. Dai, *J. Am. Chem. Soc.*, 2008, **130**, 2777.
23 Y. Pei, Y. Gao, N. Shao and X. C. Zeng, *J. Am. Chem. Soc.*, 2009, **131**, 13619.
24 D. E. Jiang, R. L. Whetten, W. Luo and S. Dai, *J. Phys. Chem. C*, 2009, **113**, 17291.
25 D. E. Jiang, W. Chen, R. L. Whetten and Z. Chen, *J. Phys. Chem. C*, 2009, **113**, 16983.
26 Y. Pei, Y. Gao and X. C. Zeng, *J. Am. Chem. Soc.*, 2008, **130**, 7830.
27 D. E. Jiang, *Chem.–Eur. J.*, 2011, **17**, 12289.
28 N. K. Chaki, Y. Negishi, H. Tsunoyama, Y. Shichibu and T. Tsukuda, *J. Am. Chem. Soc.*, 2008, **130**, 8608.
29 D. E. Jiang, M. Walter and J. Akola, *J. Phys. Chem. C*, 2010, **114**, 15883.
30 O. Lopez-Acevedo, J. Akola, R. L. Whetten, H. Grönbeck and H. Häkkinen, *J. Phys. Chem. C*, 2009, **113**, 5035.
31 M. Zhu, H. Qian and R. Jin, *J. Am. Chem. Soc.*, 2009, **131**, 7220.
32 I. L. Garzón, C. Rovira, K. Michaelian, M. R. Beltrán, J. Junquera, P. Ordejón, E. Artacho, D. Sánchez-Portal and J. M. Soler, *Phys. Rev. Lett.*, 2000, **85**, 5290; I. L. Garzón, E. Artacho, M. R. Beltrán, A. García, J. Junquera, K. Michaelian, P. Ordejón, C. Rovira, D. Sánchez-Portal and J. M. Soler, *Nanotechnology*, 2001, **12**, 126.
33 Z. Wu, M. A. MacDonald, J. Chen, P. Zhang and R. Jin, *J. Am. Chem. Soc.*, 2011, **133**, 9670.
34 M. Zhu, H. Qian and R. Jin, *J. Phys. Chem. Lett.*, 2010, **1**, 1003.
35 Y. Pei, R. Pal, C. Liu, Y. Gao, Z. Zhang and X.-C. Zeng, *J. Am. Chem. Soc.*, 2012, **134**, 3015.
36 M. J. Frisch, et al., *Gaussian 03, revision C.02*, Gaussian, Inc., Wallingford, CT, 2004.
37 D. E. Jiang, M. Walter and S. Dai, *Chem.–Eur. J.*, 2010, **16**, 4999.
38 See for example recent reports on the effect of metallophilicity on small protected gold clusters: J. Muñiz, C. Wang and P. Pyykkö, *Chem.–Eur. J.*, 2011, **17**, 368; P. Pykkö, X.-G. Xiong and J. Li, *Faraday Discuss.*, 2011, **152**, 169.
39 A. Tlahuice and I. L. Garzón, *Phys. Chem. Chem. Phys.*, 2012, **14**, 3737.
40 C. M. Aikens, *J. Phys. Chem. Lett.*, 2011, **2**, 99.
41 A. Sánchez-Castillo, C. Noguez and I. L. Garzón, *J. Am. Chem. Soc.*, 2010, **132**, 1504.
42 M. Zhu, H. Qian, X. Meng, S. Jin, Z. Wu and R. Jin, *Nano Lett.*, 2011, **11**, 3963.
43 H. Qian, M. Zhu, C. Gayathri, R. G. Gil and R. Jin, *ACS Nano*, 2011, **5**, 8935.